Journal of Alloys and Compounds 506 (2010) 703–709

Contents lists available at ScienceDirect

Journal of Alloys and Compounds

journal homepage: www.elsevier.com/locate/jallcom

Characterization and thermal modelling of friction welded alumina–mild steel with the use of Al 1100 interlayer

Hazman Seli [a], Mohamad Zaky Noh [b], Ahmad Izani Md. Ismail [c], Endri Rachman [d], Zainal Arifin Ahmad [e,*]

[a] Faculty of Computer and Mathematical Sciences, Universiti Teknologi MARA Sarawak, 94300 Kota Samarahan, Sarawak, Malaysia
[b] Faculty of Science, Universiti Tun Hussein Onn Malaysia, 86400 Batu Pahat, Johor, Malaysia
[c] School of Mathematical Sciences, Universiti Sains Malaysia, 11800 Penang, Malaysia
[d] Collaborative MicroElectronic Design Excellence Centre (CEDEC), Universiti Sains Malaysia, Engineering Campus, 14300 Nibong Tebal, Penang, Malaysia
[e] School of Materials & Mineral Resources Engineering, Universiti Sains Malaysia, Engineering Campus, 14300 Nibong Tebal, Penang, Malaysia

ARTICLE INFO

Article history:
Received 7 April 2010
Received in revised form 5 July 2010
Accepted 7 July 2010
Available online 15 July 2010

Keywords:
Friction welding
Finite difference
Intermetallic
Interface
Temperature profile

ABSTRACT

This paper reports a study of the physical and thermal behaviors of friction welded alumina–mild steel rods with the use of AL 1100 sheet as interlayer. A series of hardness tests, bending tests, macrostructure observations, SEM and EDX analyses were carried out and were combined with a finite difference thermal model to acquire material parameters. This work demonstrated the insignificant change in the hardness value of the parent alumina and the slight increase in hardness value of the parent mild steel, particularly near the interface region. The bending strength increased with the increase of friction times with the highest bending strength obtained was 186 MPa at 20 s. The fractured surface shows the strong bond at the middle of the interface. The bond was obtained through interfacial interlocking and narrow intermetallic phase formation. However, the incomplete joint observed was detrimental to the joint strength. The thermal profile predictions were compared to actual thermocouple data from welds conducted under identical conditions and were shown to be in fair agreement. Even though the FD method proposed in this study cannot replace a more accurate numerical analysis, it does provide guidance in weld parameter development and allows better understanding of the friction welding process.

1. Introduction

Joining of metal and ceramic materials by means of friction welding is possible and has been successfully performed [1–4]. Friction welding is a solid-state joining process and one of the most effective processes for joining similar and dissimilar materials with high joint integrity through the combined effects of pressure and relative motion of the two workpieces, heating of the joint interface and inducement of plastic deformation of the material. Under normal conditions, the maximum temperature at the interface is just below melting temperature. The problems concerning friction welding of dissimilar materials are not only associated with their individual properties, such as hardness and melting point, but also with the reactions that take place at the interface. Metals in general have a higher thermal expansion coefficient than ceramics. Therefore, when joining ceramics to metals using friction welding, very large thermal stresses will be induced and, in many cases, these large stresses cause joint failure. In order to overcome this problem, solid phase bonding processes have been developed in which a metallic or a composite metal–ceramic interlayer is placed between the ceramic and metal surfaces to be joined. Ceramic–metal interfaces are important in a wide range of technologies. The interfacial morphology can determine the performance characteristics of dissimilar material joints, metal–matrix composites, ceramic–matrix composites, electronic packages, glass-to-metal seals, glass processing systems, and liquid–metal processing systems. Microstructural development on ceramic–metal interfaces plays a critical role in all of these processes [5].

The analysis in the paper technological process of friction welding is applied to the end faces of two cylindrical elements made of corundum ceramics Al_2O_3 and aluminum alloy [6]. Knowledge of temperature distribution in the vicinity of the welded bond is significant in the assessment of physical processes in the area of welding. The temperature gradient and plastic thermal deformations determine microstructural changes, diffusion phenomena and mechanical properties of the finished product. Unfavourable thermal and stress effects are intensified when materials of different heat and mechanical properties, like Al_2O_3 and Al, are bonded.

Therefore it is vital to have a means of rapidly and accurately estimating peak joint temperature and cooling rate based on input parameters. A numerical code simulating the friction welding is a

* Corresponding author. Tel.: +60 4 5996167; fax: +60 4 5941011.
E-mail address: zainal@eng.usm.my (Z.A. Ahmad).

0925-8388/$ – see front matter © 2010 Elsevier B.V. All rights reserved.
doi:10.1016/j.jallcom.2010.07.047

powerful tool to tune the settings with ease and to quickly visualize the process specific responses to define the quality of the weld. In order to apply this numerical code commercially on an industrial scale, it is necessary to know the thermal phenomena that take place during the whole process and in intermediate layer creation. An analysis of these phenomena can be helpful in improving both the method and strength of the bonds.

In the literature, there are only a few papers on numerical modelling of the friction welding process. Complex papers, describing coupled thermo-mechanical phenomena in the friction welding process are mainly concerned with metals. The friction welding of similar steel rods using a coupled finite element analysis with contact conditions was modelled [7]. With this model, the distribution of temperature and the shapes of final profiles were determined [8] and presented on a FEM model of coupled deformation and heat flow analysis where the temperature, stress and strain fields for frictional welded joint of GH4169 nickel-based alloy were calculated. FEM simulation of inertia friction welding process between dissimilar materials, assuming coupling between the thermal and mechanical effects were developed [9]. The contact algorithm and elasto-viscoplastic model of material were implemented. In the mathematical modelling of temperature fields in friction welded dissimilar metals, assumption of linear pressure distribution was made on the contact surface [10] which, consequently, led to incorrect heat flux distribution on the surface and discrepancy between the temperature distribution obtained experimentally and numerically.

In this study, continuous drive friction welding was used in which the rotational motion of the workpiece is stopped after pressure has been loaded within a very short period of time (less than 2 s). During the process, the frictional heat was generated in the interface up to a maximum joint heat where plastic deformation was reached rapidly. Then the rotation was stopped to allow the welded joint to cool down freely. In friction welding, four parameters control the character of a weld: rotational speed, relative velocity between the workpieces, frictional time and axial force. These parameters determine the amount of energy input to the weld and the rate of heat generation at the interface.

The purpose of this paper is to define and analyze time–temperature profiles in bonded alumina–mild steel rods during the friction welding process with some characterizations. The FD method was applied in finding the numerical solution. The resulting temperature fields were compared with experimental data and the shortcomings of the method are discussed.

2. Method and materials

In the experimental study, rods measuring 10 mm in diameter made of alumina (50 mm length) and mild steel (50 mm length) with aluminum plate (1.4 mm thickness) interlayer were used. Their chemical compositions are listed in Table 1. The connecting surfaces of mild steel and alumina were ground to a smooth surface and the sharp edges around it were finished. The process scheme is shown in Fig. 1.

For metallurgical examination and Knoop hardness measurement, the welded sample was sectioned perpendicular to the weld interface. The successful welded samples at various friction times were also measured for their four point bending strength using Instron model 8501. The welded sample was also fractured at the joint region to investigate the fracture surface. The joint sample was ground and polished. Macrographs and micrographs were obtained using an Olympus BX51 M optical microscope and scanning electron microscope (SEM), respectively. Elements of intermetallic compounds at the interface were quantitatively detected using an Energy Dispersive X-Ray (EDX) machine. The temperature changes during the friction welding process were measured by two K-type thermocouples attached to the alumina rod (stationary) at distances of 5 mm and 10 mm from the interface.

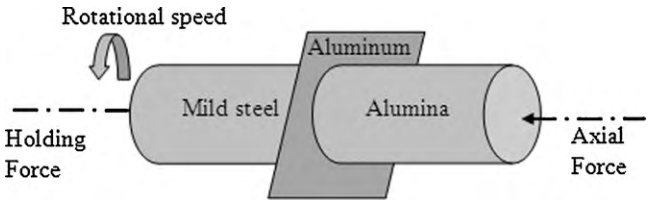

Fig. 1. Layout of continuous drive friction welding.

3. Mathematical modelling

3.1. General assumptions

For the analysis of friction welding, heat generation and pressure across the interface were assumed to be uniform. This assumption has frequently been used by many researchers in modelling friction welding. It was assumed that no heat exchange occurs between the end faces of the alumina, aluminum, mild steel rods and environment. The alumina and the steel were considered to be homogenous and isotropic. There was no heat loss through convection and radiation at the frictional interface (time short). Since the heat generated at the interfaces is very high, it was assumed that heat loss through the excess part of the aluminum piece is negligible. There were no internal heat source in both rods and the heat input was considered constant throughout the process.

3.2. Thermal analysis

In friction welding, the temperature in the weld region rises sharply due to extreme friction and plastic work of the aluminum piece within a very short time. To calculate the temperature profile, the heat transfer analysis was undertaken by considering the frictional heat generation at the interface, heat generation by plastic deformation and heat loss to the environment.

3.2.1. Frictional heat generation model

Based on the assumption that force distribution remains constant, frictional heat was deduced through the following analytical method. First, a microannulus that has an inner radius r and a width dr in the friction surface was defined as in Fig. 2.

The constant pressure acting on the entire surface is given by p. The area of the microannulus is $dA = (2\pi r)dr$. Transforming the pressure equation into a differential characterization of the area dA, the following equation is obtained for the differential force, dF, acting on the area dA.

$$dF = pdA = 2p\pi rdr \quad (1)$$

Since dF is equivalent to the equal and opposite normal force acting on dA, the differential frictional force, dF_f, can be specified as

$$dF_f = \mu dF = 2\mu p\pi rdr \quad (2)$$

Table 1
Chemical composition of mild steel, alumina and aluminum.

	Composition (wt%)												
	C	Si	P	S	Cr	Mn	Ni	Al	Cu	Fe	Mg	O	Bal
Mild steel	0.30	0.22	0.02	0.02	0.12	0.78	0.10	–	0.44	98	–	–	<0.01
Alumina	–	–	–	–	–	–	–	52.71	–	–	–	47.28	<0.01
Aluminum	–	0.59	–	–	–	0.09	0.01	98	0.25	0.22	0.85	–	<0.01

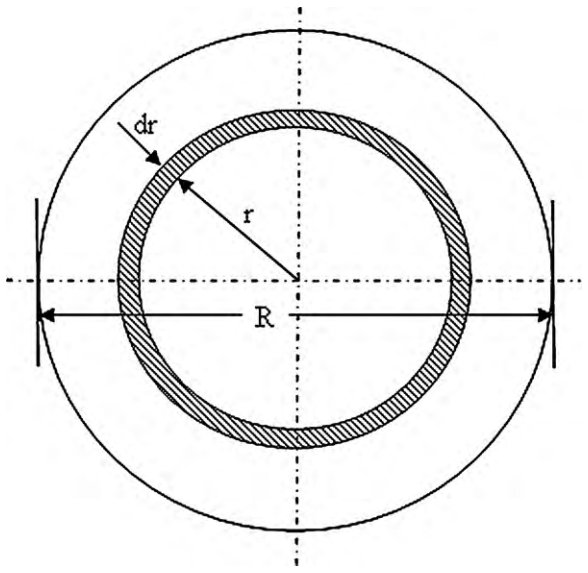

Fig. 2. Friction interface sketch.

where, μ is friction coefficient. It is known that the tangential velocity, v_T at any point on the element is the same,

$$v_T = r\omega \tag{3}$$

where, ω is angular velocity. The differential power that is exerted to rotate the annulus area dA is

$$dP = dF_f(v_T) = 2\mu p\pi r^2 \omega dr \tag{4}$$

Therefore, by integrating Eq. (4) with respect to r, the definition for the frictional heating power generation is obtained as

$$P = \int_0^R 2\mu p\pi r^2 \omega \; dr = \frac{2}{3}\mu p\pi R^3 \omega \tag{5}$$

The heat flux (q) generated by friction at the annulus is given as

$$q(r) = \frac{dP}{dA} = \mu p \omega r \tag{6}$$

3.2.2. Plastic deformation heat source

The temperature change during material deformation will induce its physical and mechanical properties. In material deformation analysis, the constitutive relationship between material and its thermal strain will change under the influence of temperature distribution during the heat transfer process where the material deformation will change the heat transfer space, the boundary conditions and the energy transition.

The plastic deformation power or the internal energy rate, $\dot{q}$, in the ductile material away from the interface can be defined as

$$\dot{q} = \beta\bar{\sigma}\dot{\bar{\varepsilon}} \tag{7}$$

where, $\bar{\sigma}$ is the equivalent stress, $\dot{\bar{\varepsilon}}$ is equivalent strain rate and β is the thermal efficiency of plastic deformation. According to the theory of plastic deformation, most of plastic deformation work transforms to heat with the thermal efficiency, β typically set as 0.9 [8]. The rest of the energy is principally stored as dislocations and vacancies. For the benefit of simplicity in the computation, this internal energy rate was neglected due to its low value compared to the frictional heat generation.

3.3. Heat transfer

The schematic weldment for the calculation is shown in Fig. 3. The fundamental non-steady equation of Fourier's heat conduction

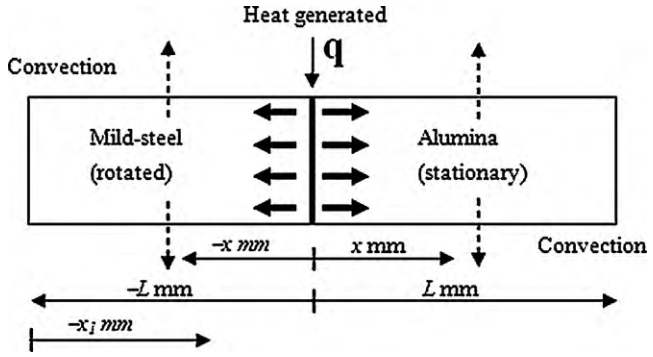

Fig. 3. Boundary conditions used for the model.

in the coupled thermo-mechanical problem can be expressed as follows:

$$\frac{\partial T}{\partial t} + u\frac{\partial T}{\partial x} = \frac{1}{\rho C_p}\frac{\partial}{\partial x}\left(k\frac{\partial T}{\partial x}\right) - \frac{hP}{\rho C_p A}(T - T_o) + \dot{q} \tag{8}$$

where, T is temperature, T_o is the ambient temperature around the rod, u is the shortening velocity, ρ is the material density, C_p is the specific heat capacity, A is the cross-sectional area, P is the perimeter of the rod, k is the thermal conductivity, h is the convection coefficient, x is the distance from the weld interface and t is time.

For simplicity, Eq. (8) can be rewritten

$$\frac{\partial T}{\partial t} + u\frac{\partial T}{\partial x} = \alpha\frac{\partial^2 T}{\partial x^2} - \beta(T - T_o) + \dot{q} \tag{9}$$

where

$$\alpha = \frac{k}{\rho C_p} \quad \text{and} \quad \beta = \frac{hP}{\rho C_p A}$$

In this one-dimensional transport equation, the convection term on the right-hand side of the equation accounts for heat conduction and heat lost through convection along the lateral surfaces of the two components. It is assumed that there is no heat lost through radiation at the frictional interface. The problem of heat conduction in the whole process of friction welding determined by means of Eq. (9) is, thus, simplified to the calculation of temperature field, $T = T(x,t)$. The calculation of the temperature of the friction welding process is carried out in two stages. The first stage is the heating part while the second is the cooling process. Fig. 3 shows the boundary conditions used for the model. The initial and boundary conditions when solving Eq. (9) are expressed based on the two stages.

The initial and boundary conditions when solving Eq. (3) are expressed based on the two stages.

3.3.1. Heating stage

The heating temperature distribution is calculated separately for the two equal length (L) rods by assuming common average heat generated at the interface. For the heating stage, the initial and boundary conditions for the simplified Eq. (9) are derived as

$$T(x, t_h) = T_o \quad \text{for} \quad t_h = 0 \tag{10}$$

$$-k\frac{\partial T}{\partial x} = q, \quad x = 0 \quad \text{for} \quad t_h > 0 \tag{11}$$

and

$$-k\frac{\partial T}{\partial x} = h(T - T_o), \quad x = L \quad \text{for} \quad t_h > 0 \tag{12}$$

where, t_h is the heating or frictional time. T_o is the initial temperature of the specimen which is taken as 29 °C, q is the surface heat flux generated at the friction surface ($x = 0$).

Table 2
Material data used in calculations [10].

Properties	Alumina	Mild steel
Density, kg m^{-3}	3950	7800
Heat transfer coefficient, W m^{-2} K^{-1}	20	20
Thermal conductivity, W m^{-1} K^{-1}	16.7	43
Specific heat capacity, J kg^{-1} K^{-1}	950	470

3.3.2. Cooling stage (welded)

At this stage, the rods have been joined and are considered as one new rod ($2L$) in the calculation where the initial and boundary conditions for the simplified Eq. (9) are derived as

$$T(x_j, t_c) = T_n \quad \text{for} \quad t_c = 0 \tag{13}$$

$$k_s \frac{\partial T}{\partial x} = h_s(T_s - T_o), \quad x_j = 0 \quad \text{for} \quad t_c > 0 \tag{14}$$

and

$$-k_a \frac{\partial T}{\partial x} = h_a(T_a - T_o), \quad x_j = 2L \quad \text{for} \quad t_c > 0 \tag{15}$$

where, x_j is the distance from left end of the joined rods, t_c is the cooling time, k_s and k_a are the thermal conductivity of the mild steel and the alumina, respectively and T_s and T_a are the temperature of the free surfaces of the mild steel and the alumina, respectively. T_n is the last temperature profile from the previous heating stage with n final time step. In this paper, numerical solutions based on the finite difference method were utilized. The only unknown in the FD model presented above is the shortening velocity which is assumed to be zero. The FD model for temperature profiles of this process was set up based on MATLAB software package.

The flowchart of the algorithm is presented in Fig. 4. The thermal properties of mild steel and alumina from www.matweb.com are listed in Table 2.

4. Results and discussion

The friction welding process was done on a continuous drive friction welding machine. The friction welding conditions were 900 rpm rotational speed, 20 MPa axial pressure and 3.2 s frictional time. Hardness profiles of the welded sample were determined. Interfaces of the welded sample were observed and analyzed. The calculation of the temperatures was carried out using MATLAB software package.

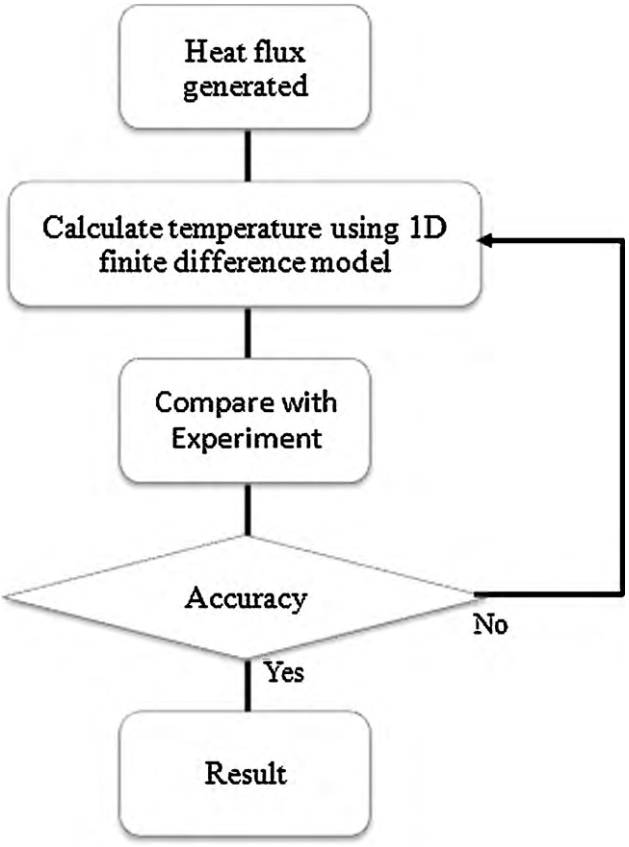

Fig. 4. Flowchart of the temperature calculation.

4.1. Friction welded joint characterization

4.1.1. Hardness profiles

The hardness profile near the bondline of the alumina–mild steel joint is shown in Fig. 5. The hardness profile in the alumina part exhibited insignificant change and remained constant with before the friction process, i.e. within the range of 1000–1300 KHN. Because alumina has inert, hard and brittle properties, only aluminum atom diffusion occurs at the contact surface during the friction process. On the other hand, the hardness value for the mild steel part slightly increased towards the joint (reaching 200 KHN). This resulted from the effects of the formation of the narrow brittle intermetallic phase at the mild steel–aluminum interface, as discussed in the interfacial microstructure characterization.

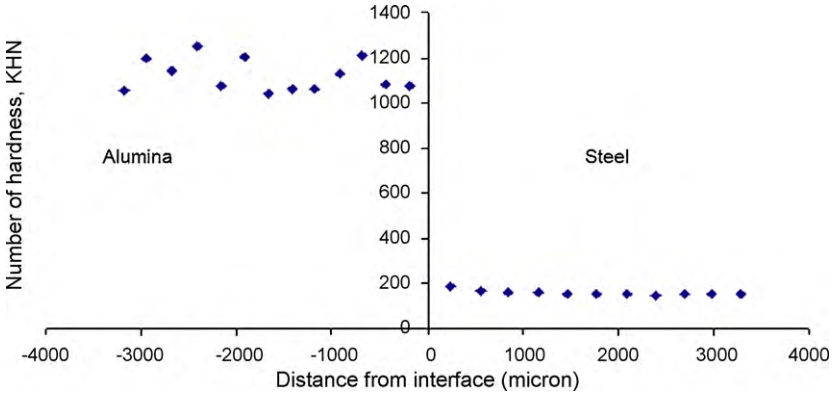

Fig. 5. Result of microhardness test of alumina–mild steel joint.

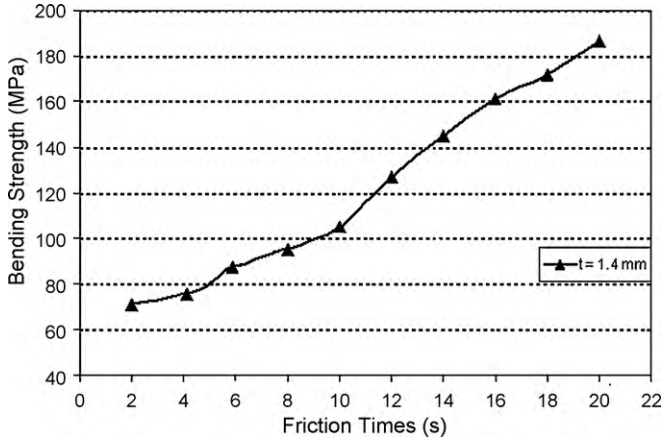

Fig. 6. Bending strength versus various friction times at rotational speed of 900 rpm.

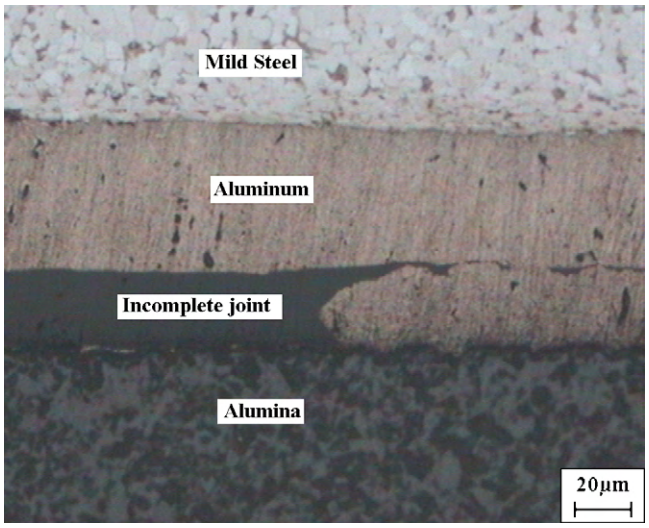

Fig. 7. Micrograph of two interfaces of mild steel–aluminum and alumina–aluminum with incomplete joint.

4.1.2. Bending strength

Fig. 6 shows the correlation between friction times and bending strength of the mild steel–alumina joint. The strength of the joint is dependent on the friction time of the process. The bending strength increased with the increase of friction times. The highest bending strength was observed at the friction time of 20 s with 186 MPa. The trend is due to the longer friction time that produced excessive generated heat and provided large deformation of aluminum interlayer which allows sufficient welding and interlocking for bond formation. Under the shorter duration of friction times, the generated heat obtained was not enough to diffuse the aluminum interlayer and the thickness becomes thicker. In addition, an incomplete joint could also exist due to lower friction times.

4.1.3. Interfacial microstructure analysis

The SEM evaluation revealed some significant facts that are shown in Fig. 7. The interfacial microstructure of mild steel–aluminum interface and alumina–aluminum interface with incomplete joint are obviously observed. The bonding occurs at the interfaces by mechanical mixing and interlocking mechanism whenever plasticized aluminum atom diffuses into the mild steel and alumina surfaces. Mechanical mixing and interlocking at the mild steel–aluminum interface are seen to be better than at the alumina–aluminum interface. The incomplete joint used to exist at the alumina–aluminum interface when the joining process was

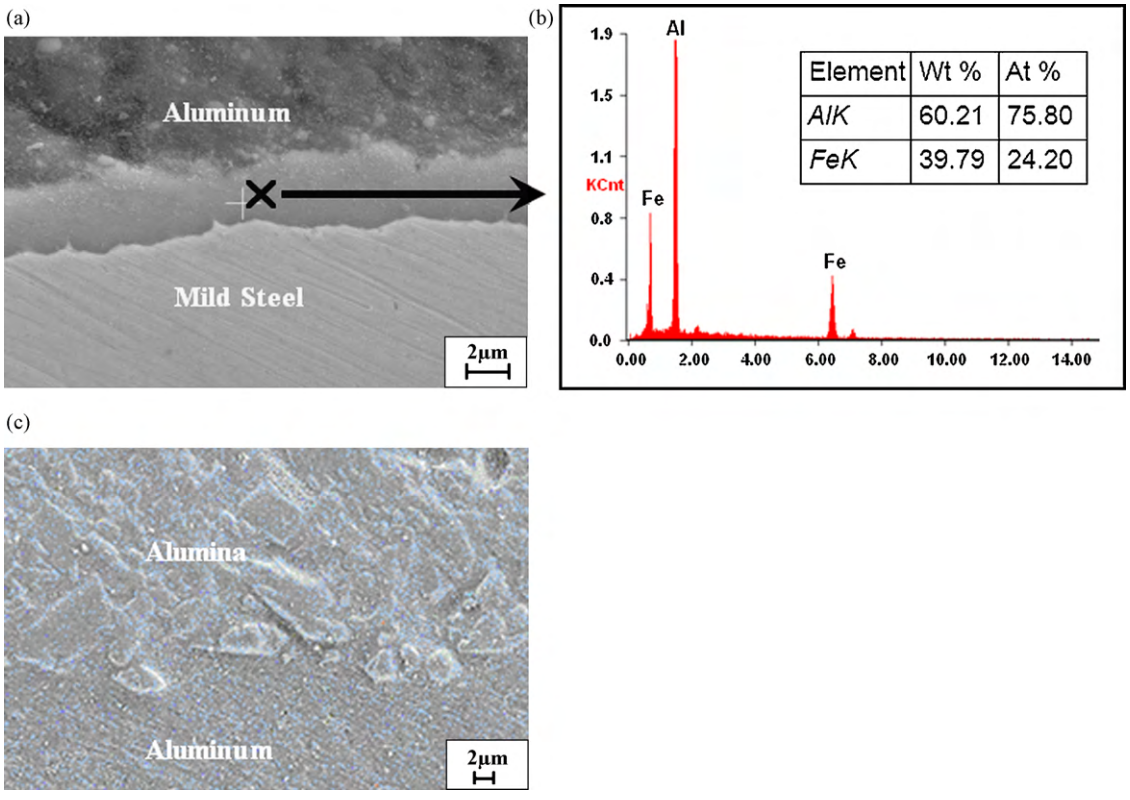

Fig. 8. (a) The formation of intermetallic compound ($FeAl_3$) at the interface area of mild steel–aluminum, (b) EDX analysis of the intermetallic compound and (c) interlocking at the alumina–aluminum interface.

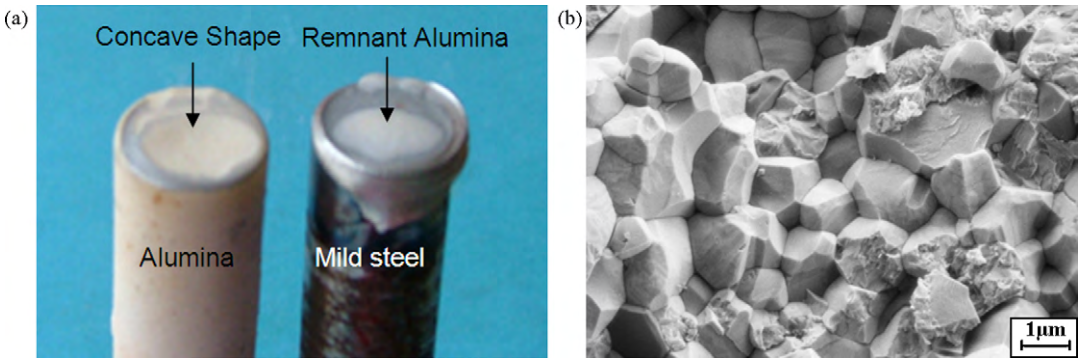

Fig. 9. (a) The fracture surfaces of the alumina–mild steel interface joint and (b) the existing pores in the alumina rod.

repeated. The incomplete joint occurs due to major differences in melting points and higher surface energy in alumina–aluminum interface compared to that of mild steel–aluminum interface.

The friction process of dissimilar metals may produce an intermetallic region at the interface area [11]. Fig. 8a shows an enlarged interfacial microstructure of mild steel–aluminum with the presence of a very narrow intermetallic compound. The intermetallic phase was clearly detected by EDX analyzer (Fig. 8b) as a combination of the following elements, 60.21 wt% Al and 39.79 wt% Fe ($FeAl_3$). This compound is brittle and could be detrimental to the joint strength if its formation is not controlled. Longer duration of the friction process could produce more intermetallic compounds [12]. Therefore, controlling friction time could limit the growth of the intermetallic phase at the mild steel–aluminum interface. Normally, a very short friction time (less than 2 s) is attempted to avoid wider intermetallic phase formation. On the other hand, the alumina–aluminum interface, as illustrated in Fig. 8c, does not show the presence of new phase except the mechanical interlocking of alumina and aluminum. Alumina is a very stable ceramic and it only allows reactions to occur at higher sintering temperatures (1600 °C).

4.1.4. Interfacial fracture analysis

Fig. 9 shows a macrograph of a small concave shape of fractured alumina–aluminum interface on the alumina contact surface. A small remnant of the alumina part was fractured and remained intact at the aluminum interlayer as shown in Fig. 9a. It shows that there is sufficient diffusion of softened aluminum atom in the alumina surface to create a bond. This alumina remnant is normally obtained at the center of the fractured joining samples. The highest temperature and pressure are reached in the region located in the middle part of the radius of the bonding zone [13]. The alumina–aluminum interface bond is stronger than the alumina bond as the fracture occurred in the alumina part. The fracture is due to the existing pores in the alumina rod which induce microcracks to propagate whenever under the influence of fractural load. Fig. 9b shows the micrograph of the existing grains and pores of the fracture surface of the alumina rod.

4.2. Heating profile

The estimated heating temperature distribution of the welding zone at 0.96 s, 1.92 s and 3.2 s are shown in Fig. 10. The temperature is very high near the frictional interface and the gradient of the temperature is very steep in the axial direction. As a result, the heat affected zone is very narrow. Due to this, mild steel has a narrower heat affected zone compared to alumina. It can be seen from the distribution that the calculated peak heating temperature at 3.2 s is about 442 °C with constant heat generated. The temperature reaches the peak value but does not exceed the melting point of aluminum, i.e. 660 °C. This is because of the interaction between the frictional heating power and the frictional characteristics on the surface.

The predicted heating profiles show non-symmetrical curves on both sides of the joined rods based on their thermal properties difference. The predicted temperature increases rapidly at the interface, and gradually towards the ends of the two rods. The temperature profile in mild steel is broader and is expected to have faster heat transfer. This is due to the higher thermal conductivity value in mild steel compared to that in alumina as stated in Table 2. The thermal heating profile likely exhibits the frictional characteristics on the interface. However in a real situation, the pressure distribution is not uniform with time as the two workpieces move in sinusoidal fashion. While the axial force remains constant, the area of contact between the two workpieces changes with movement, thus the axial pressure oscillates in turn. Therefore, alteration of the axial pressure during every cycle owing to the variation of contact area causes the frictional heat input to fluctuate as well. The friction coefficient varies widely with temperature. The increase in the temperature brings about deep ploughing to alter into polishing and the friction coefficient is dramatically reduced. The inaccuracy in the calculation was attributed to the assumption of constant coefficient of friction and pressure for the analytical constant heat generation.

4.3. Cooling profile

The cooling temperature profiles for the chosen cooling times 3.2 s, 4.16 s, 5.12 s and 6.4 s are shown in Fig. 11.

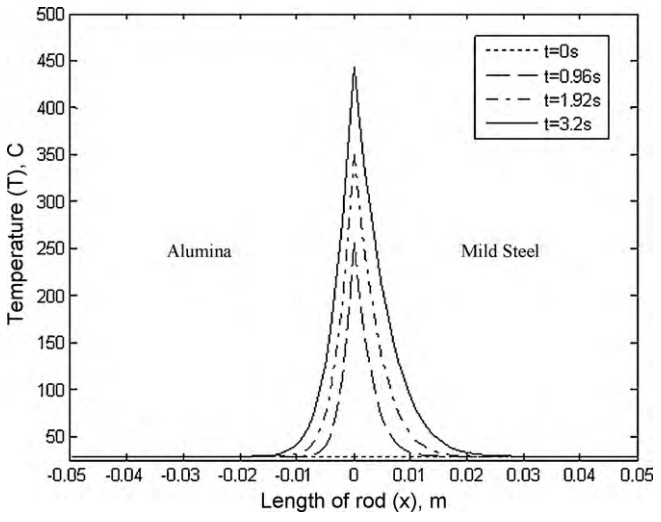

Fig. 10. The heating temperature distribution of friction welding process up to 3.2 s.

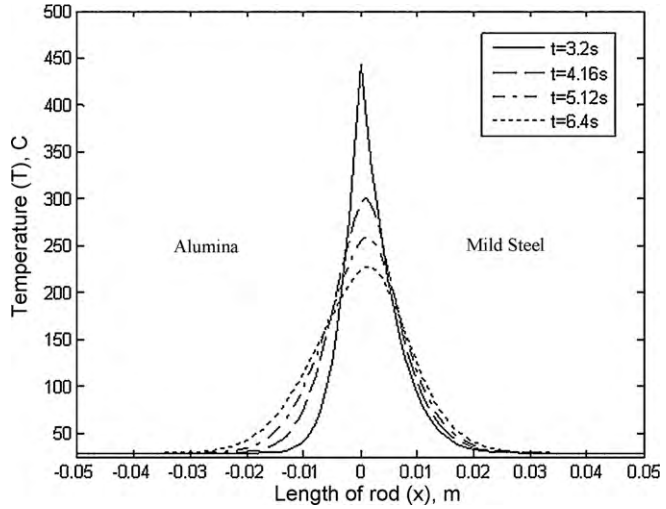

Fig. 11. The cooling temperature distribution of friction welding process after 3.2 s.

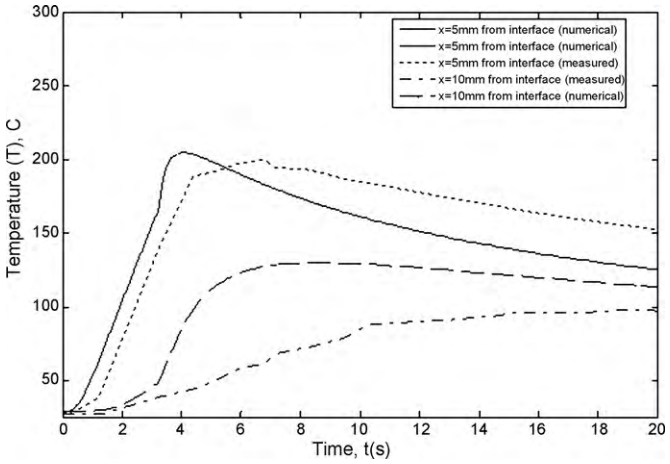

Fig. 12. Time–temperature profile at distance of 5 mm and 10 mm from the weld interface for numerical and experimental data.

The cooling starts at 3.2 s of the entire process where the last heating temperature profile was utilized. The cooling profiles shown are different from the heating profiles where the heat spreads towards the ends of the rods, making the lower temperature profiles broader. This phenomenon occurs due to the different thermal properties. Alumina has lower thermal conductivity and higher specific heat compared to that of mild steel. Therefore, it has broader cooling profiles.

4.4. Verification of FD model

The verification of the predicted temperature distribution of the welded alumina rod is presented in Fig. 12 for locations 5 mm and 10 mm from the interface. The computed temperature profile does not generally match the experimental data due to some errors, particularly the cooling part. However, the trend of the two profiles shown is almost the same. Therefore, the predicted cooling temperature profiles of the friction welding are in fair agreement with the experimental temperature profiles.

The calculated peak heating temperature at locations 5 mm and 10 mm from the interface are 204.5 °C and 129.9 °C for cooling times 4.03 s and 8.03 s, respectively. For the first numerical profile (5 mm), right after 3.2 s (flywheel rotation stopped), the temperature was still increasing till up to 204.5 °C and then dropped gradually and consistently decreased to room temperature. The numerical and experimental heating and cooling rates of the process are almost identical and approximately calculated around 50.87 °C/s and 6.23 °C/s, respectively. On the other hand, the second numerical profile (10 mm) when compared to the experimental profile showed an obviously different trend. The numerical profile indicates the heating part continued for 8 s, while the experimental profile indicated a very long heating time that went beyond 20 s. The discrepancy of the two temperature profiles is mostly attributed to the static nature of the model. The difference is quite significant, most probably because the proposed model does not consider the entire workpieces for the calculation.

In the friction welding process, at every moment of the friction phase, the plasticized material is expelled out of the faying surface due to the mutual movement of the mating surfaces. In contrast, the preliminary FD model is simply based on the static analysis in which the heat generated at the interface is assumed to be totally transferred to the base materials with no flash formed (zero axial shortening assumption). Therefore, the relative movement (rubbing) of the two parts, which is the main reason for ejecting softened material from the rubbing surface, is not considered in the model. Apart from that, the errors could also have come from the temperature measurement since the operation was manual. Nevertheless, the preliminary proposed model provides some parameter improvement and allows better understanding for further progress in developing the friction welding process.

5. Conclusions

Bonds of alumina and mild steel were achieved through interfacial interlocking and narrow intermetallic phase formation during friction welding process. The strong bond in the middle of the interface shown by the fractured surface was observed to be an incomplete bond. The insignificant change in hardness value of the parent alumina and slight increase in hardness value of the parent mild steel, particularly near the interface region, were demonstrated. The highest bending strength was observed at the friction time of 20 s with 186 MPa. A one-dimensional FD numerical model for continuous drive friction welding was developed according to the characteristics of friction welding process to enable a better understanding of the process. The predicted temperature profiles of the friction welding are in fair agreement with the experimental temperatures.

Acknowledgements

The authors gratefully acknowledge the financial support of this work by Universiti Teknologi MARA (UiTM), Universiti Sains Malaysia (USM) and Ministry of Higher Education, Malaysia.

References

[1] C. Dawes, Joining of Ceramics by Friction Heating and Forging, TWI, 2001.
[2] S. Jones, Can Ceramics be Friction Welded to Metals? TWI, 2003.
[3] C. Dawers, Joining of Ceramics by Friction Heating and Forging, TWI, 2001.
[4] W. Włosi'nski, T. Chmielewski, Welding Review 12 (2003) 1–15.
[5] A. Meier, D.A. Javernick, G.R. Edwards, JOM (1999) 44–47.
[6] J. Zimmerman, W. Wlosinski, Z.R. Lindemann, Journal of Materials Processing Technology 209 (2009) 1644–1653.
[7] A. Sluzalec, International Journal of Mechanical Sciences 32 (1990) 467–478.
[8] L. Fu, L. Duan, Welding Journal 77 (1998) 202–207.
[9] L.D. Alvise, E. Massoni, S.J. Walloe, Journal of Materials Processing Technology (2002) 387–391.
[10] A. Ambroziak, Advances in Manufacturing Science and Technology 26 (2002) 39–54.
[11] M. Yilmaz, M. Çöl, M. Acet, Materials Characterization 49 (2002) 421–429.
[12] S. Fukumoto, H. Tsubakino, K. Okita, M. Aritoshi, T. Tomita, Scripta Materialia 42 (2000) 807–812.
[13] J. Zimmerman, Welding International 20 (2006) 457–461.